

# Enhanced structural and optical properties of Mn-doped BiFeO<sub>3</sub> nanoparticles at different substitutions

M. SAJJAD<sup>a</sup>, S. ASLAM<sup>a</sup>, K. ALI<sup>a\*</sup>, Y. JAMIL<sup>a</sup>, H. M. KHAN<sup>e</sup>, M. R. AHMAD<sup>b</sup>, M. Z. RASHID<sup>c</sup>, M. ALZAID<sup>d</sup>

<sup>a</sup>Nano-optoelectronics Research Laboratory, Department of Physics, University of Agriculture Faisalabad, 38040 Faisalabad, Pakistan

<sup>b</sup>Centre for Advanced Studies in Physics (CASp) GC University Lahore, Pakistan

<sup>c</sup>Horticultural Research Institute, Ayub Agricultural Research Institute, Faisalabad, Pakistan

<sup>d</sup>Physics Department, College of Science, Jouf University, P.O. Box 2014, Al-Jouf, Sakaka, Saudi Arabia

<sup>e</sup>Institute of Physics, Islamia University of Bahawalpur, Bahawalpur, Pakistan

BiFeO<sub>3</sub> is a multiferroic substance which exhibits both antiferromagnetic and ferroelectric behaviour. Manganese doped Bismuth ferrite (BiFeO<sub>3</sub>) nanoparticles were prepared by using co-precipitation method, BiFeO<sub>3</sub> was fabricated with the substitution of manganese from 10%, 20%, 30%, 40% and 50%. However, a small lattice distortion or phase change appeared due to shifting of peaks to the higher angle in bismuth ferrite samples, it also enhances the Mn content. The crystal structure, average crystallite size, hkl planes, lattice constant and volume of unit cell were analyzed by using XRD. We demonstrate that the value of lattice constant “a” increased while volume of unit cell gradually decreases, however, average crystallite size changed irregularly. Results accomplished by SEM are illustrated to observe the change in composition of the samples by variation of manganese concentration. The optical characteristics of the prepared specimen have been measured using UV-Vis spectroscopy. The wavelength range of absorption spectrum is found in between 378nm to 385nm. The magnitude of I – V curve gradually decreases on further increment of dopant element.

(Received August 13, 2020; accepted April 8, 2021)

**Keywords:** Optical properties, Morphology, Magnetoelectric devices, Substitution

## 1. Introduction

Multiferroic materials become center of interest in several areas of physics due to potential applications in design of magneto-optical and magnetoelectric devices. Moreover, these materials having coupling between ferromagnetic and ferroelectric orders [1]. Indeed, externally applied electric and magnetic fields causes a change in magnetization and ferroelectric character respectively. These variations would leads to technological innovations in development of storage medias with magnetic reading, ferroelectric writing [2] and spintronics [3]. The co-existence and coupling with elasticity provide an extra degree of freedom to design multistage devices. These orders hardly coexist in nature due to 3D electronic orbital structure and d<sup>0</sup> electronic structure of B-sites elements. As the ferroelectric materials shares approximately same crystal structure. Typical ferroelectric substance has cubic ABO<sub>3</sub> perovskite parental phase. In which A-site cation has stereochemical active 6s<sup>2</sup> lone pair which are off-centered by low energy electrons sharing between empty 6p orbitals and filled O 2p orbitals, while B-sites cation has empty d-shell (d<sup>0</sup>) electronic configuration. There are few naturally occurring single phase perovskite oxides such as YMnO<sub>3</sub>, BiMnO<sub>3</sub> and BiFeO<sub>3</sub> which possess spin and ferroelectric order above room temperature, Therefore, these materials propose fundamental applications in information storage,

converters, sensors, photo catalyst [4, 5] multi-functional electronic devices [6], which acquire the attention of researchers. BiFeO<sub>3</sub> (BFO) is an appealing single-phase Multiferroic material having high ferroelectric curie temperature (~ 820°C) and G-type antiferromagnetic Neel temperature (~ 360°C). Lone pair of electrons of Bi<sup>3+</sup> are responsible to produce ferroelectric orders whereas unpaired Fe spins produce ferromagnetic orders. The antiferromagnetic is complex due to spin coating and long-range spin cycloid formation which incommensurate with lattice [7]. BFO possess a distorted perovskite rhombohedral crystal structure having R3c space group. BFO is well known for its wide range of applications in spintronic devices [8]. By the virtue of small band gap energy, BFO covers wide sunlight spectrum which make it favorable for photo-catalytic activity and photo-induced applications. The studies have shown that ions doping at A-sites, B-sites or at A-B-sites of BFO enhances its optical and multiferroic properties as well as overcome problem of leakage current density [7]. For doping rare earth ions like Nd, La, Pr and Gd doped at A-sites of BFO helps to reduce leakage density (due to decrease in oxygen vacancies) whereas B-sites of BFO doped with transition metal ions like Co, Rh, Ru and Cu effectively enhance magnetoelectric characteristics [9]. In the present work, bismuth ferrites were prepared by the doping manganese to bismuth sites with different concentrations. There are various techniques that are available for the preparation of

Mn-doped BiFeO<sub>3</sub>. Co-precipitation is a very economical and efficient process with the benefit of low-temperature concretization [10]. Bismuth ferrite powder samples were prepared with the co-precipitation technique from 10% to 50% of Manganese content. The crystal structure, average crystallite size, lattice constant "a," volume of the unit cell, morphology, and absorption spectrum were observed by using XRD, SEM, and UV-Vis spectroscopy.

## 2. Experimental details

Co-precipitation technique was used to synthesize powder mixture of manganese doped BiFeO<sub>3</sub>, at low temperature (80°C). The commercial grade bismuth oxide (Bi<sub>2</sub>O<sub>3</sub>) and the analytical grade Iron nitrate nonahydrate Fe (NO<sub>3</sub>)<sub>3</sub>.9H<sub>2</sub>O were used as precursors. These powders were weighted by their required stoichiometric values. Both Bi<sub>2</sub>O<sub>3</sub> and Fe (NO<sub>3</sub>)<sub>3</sub>.9H<sub>2</sub>O powders were dissolved into nitric acid (HNO<sub>3</sub>) and water to form 0.1 M solution. The 1mM solution was obtained in distilled water with the manganese chloride tetrahydrate (MnCl<sub>2</sub>.4H<sub>2</sub>O). As precipitating agent, we use an aqueous solution of 1.0 M Sodium Hydroxide (NaOH). The Fe (NO<sub>3</sub>)<sub>3</sub>.9H<sub>2</sub>O and Bi<sub>2</sub>O<sub>3</sub> solution were liquidated into a different beaker. The calculated amount of MnCl<sub>2</sub>.4H<sub>2</sub>O was mixed in bismuth oxide solution. Now combine this solution with Iron nitrate solution and put the collective mixture on magnetic stirrer. Sodium hydroxide (NaOH) solution was used to pour down to resultant solution in an effective manner. After vigorous mixing for about 30 min till pH of 7 was achieved, leave the solution mixture in water bath for about 45 min at 80°C to transform hydroxides into ferrites. The subsequent product was dried in an electric oven at 80°C, then grind precisely to transform it in a fine amorphous powder. For crystallization the powder was placed in the furnace to calcination for one hour at 200°C. Bismuth nitrate is usually used as precursors in the co-precipitation process for the Mn-doped BiFeO<sub>3</sub> synthesis, however bismuth oxide (Bi<sub>2</sub>O<sub>3</sub>) and iron nitrate nonahydrate (NO<sub>3</sub>)<sub>3</sub>.9H<sub>2</sub>O were used as precursors in this work. Bismuth nitrate pentahydrate Bi (NO<sub>3</sub>)<sub>3</sub>.5H<sub>2</sub>O and (Bi<sub>2</sub>O<sub>3</sub>) requires acid to liquified instead of distilled water. Whereas, iron nitrate nonahydrate Fe (NO<sub>3</sub>)<sub>3</sub>.9H<sub>2</sub>O can directly dissolve in distilled water. The phase identification and complete structural analysis of the powder specimens were examined using XRD with Cu K $\alpha$  radiation source. The average crystallite size and morphology were observed by using SEM. The optical properties were analyzed by UV-Vis spectroscopy.

## 3. Results and discussion

Fig. 1 illustrates the XRD patterns of extracted and calcinated BFO specimens with content of [Mn]=10,20,30,40 and 50% The findings have shown that BiFeO<sub>3</sub> samples had perovskite-based rhombohedral structure and no other impurity phase was present up to 30% but at 40% small impurities were present [10] but

the structure phase unchanged. As dopant element (Mn) starts increasing from 30% to 50%, the peak (104) was shifted to larger angles, whereas the peak (110) was approximately changed. At the Mn concentration of 40% and 50% these merged to a single (110) peak and shifted from lower angle to higher angle. The results showed that the rhombohedral structure of bismuth ferric oxide with an increasing content of Mn has small distortions [11]. The unknown peak is observed in Fig. 1. The peak is not identified for pure BFO, however distortions in peak positions are attributed towards modification of 20% Mn.

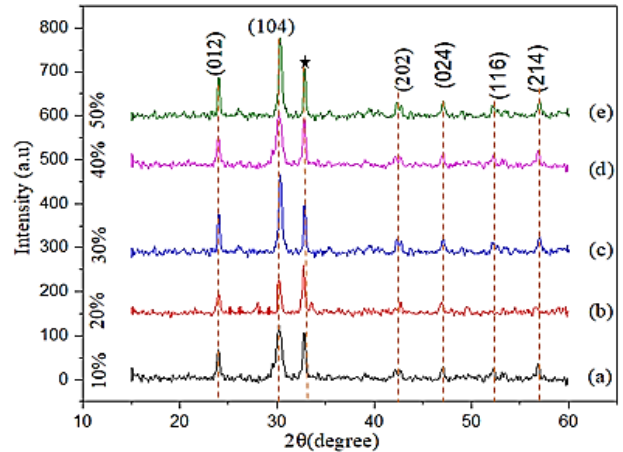


Fig. 1. XRD patterns of BFO having Mn Content (a)10% (b) 20% (c) 30% (d) 40% (e)50% (color online)

All peaks were matched with standard JCPDS card (JCPDS card no. 20-0169). The sample cell volume and lattice parameters were measured. At different concentrations of Mn, the Lattice constant is decreases due to the larger ionic radii of (Fe<sup>+</sup>) and unit cell volume. Particle size of samples was measured using Scherrer's formula with full width half maximum (FWHM).

$$D = \frac{0.9\lambda}{\beta \cos \theta} \quad (1)$$

By using following formula lattice parameters can be calculated

$$\frac{1}{d^2} = \frac{(h^2+k^2+l^2) \sin^2 \alpha + 2(hk+kl+hl)(\cos^2 \alpha - \cos \alpha)}{a^2(1-3 \cos^2 \alpha + 2 \cos^3 \alpha)} \quad (2)$$

where "d" is the d-spacing or interplanar distance and "hkl" represents miller indices.

Fig. 2 shows Mn concentration against crystalline size and Lattice constant of BFO. Owing to the fact that the lattice constant decreases due to the lower ionic radius (0.645 Å) of Mn<sup>2+</sup> relative to the ionic radius of Fe<sup>3+</sup> (0.782 Å), the merged peak in Fig. 1 moves towards a higher angle. The Mn content begins to take host lattice dimension and interstitial sites starts to expand when Mn concentration reaches to 50% or higher. Fig. 2 illustrates the average crystalline size decreases with increasing the Mn concentrations this may be attributed towards growth

of crystal restricted by the substitution element with different ionic radii.

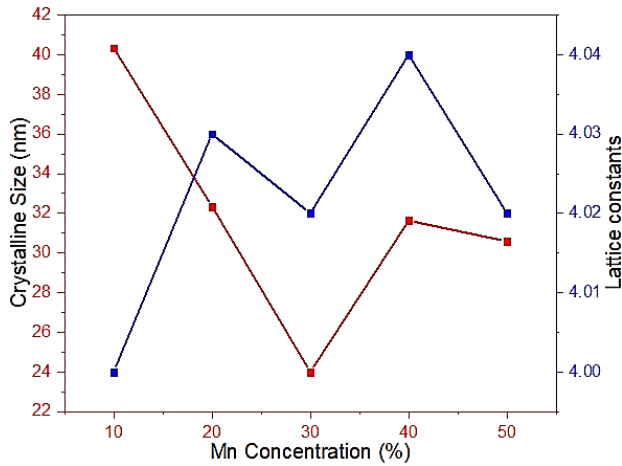


Fig. 2. Graph plotted of Mn concentration against crystalline size and Lattice constant of BFO (color online)

Volume can be calculated from given formula

$$v = a^3(1 - 3 \cos^2 \alpha + 2 \cos^3 \alpha)^{\frac{1}{2}} \quad (3)$$

Strain can also be calculated from given formula

$$\text{strain} = \frac{k\lambda}{D} \quad (4)$$

where  $\lambda$  is the x-ray incident wavelength ( $\lambda = 1.5406 \text{ \AA}$ ), B is the full width at half maximum (FWHM) and  $\theta$  is the angle of diffraction.

Density can be measured by the following formula

$$\text{Density } (\rho) = \frac{nMw}{N_A V} \quad (5)$$

where n is the number of atoms per unit cell, Mw is the molecular weight,  $N_A$  Avogadro number and its value is  $6.02214076 \times 10^{23}$ , V is the volume of unit cell.

Dislocation density has been determined by the following relation.

$$\text{Dislocation density } (\rho) = \frac{1}{D^2} \quad (6)$$

where "ρ" is the dislocation density and "D" is the average crystalline size.

Here, we can calculate the number of unit cell from the following equation

$$n = \pi \times \left(\frac{4}{3}\right) \times \left(\frac{D}{2}\right) \times \left(\frac{1}{V}\right) \quad (7)$$

where "n" is the number of unit cell, "D" is the average crystalline size and "V" is the volume of the unit cell. Morphology index can also be calculated from the following relation

$$M.I = \frac{FWHM_h}{FWHM_h + FWHM_p} \quad (8)$$

where (M.I) is morphology Index,  $FWHM_h$  is the high peak and  $FWHM_p$  is the particular peaks.

From Fig. 2, the particles size of the samples was found to be 40.34nm, 32.35nm, 24.00nm, 31.63nm and 30.59nm for Mn-10% doped BFO, Mn-20% doped BFO, Mn-30% doped BFO, Mn-40% doped BFO and Mn-50% doped BFO respectively.

Table 1. Lattice parameters of Mn doped BFO ferrites

Mn content (%)	Average particle size (nm)	Lattice constant ( $\text{\AA}$ ) a = b = c	Volume of unit cell (V)	Density ( $\rho$ )	Dislocation density ( $\rho$ )	Number of atom (n)	Morphology Index (M.I)
10	40.34	4.00	40.13	$1.66 \times 10^{-23}$	$6.1 \times 10^{-4}$	2.1	0.70
20	32.35	4.03	41.04	$1.6 \times 10^{-23}$	$9.5 \times 10^{-4}$	1.65	0.67
30	24.00	4.02	40.73	$1.64 \times 10^{-23}$	$1.7 \times 10^{-4}$	1.23	0.83
40	31.63	4.04	41.34	$1.6 \times 10^{-23}$	$10 \times 10^{-4}$	1.6	0.75
50	30.59	4.02	40.73	$1.64 \times 10^{-23}$	$1.07 \times 10^{-4}$	1.57	0.83

Fig. 3 illustrates that Mn concentration is increases from (10% to 50%) the Lattice constant is decreases due to the larger ionic radii of ( $\text{Fe}^{+3}$ ).

This is may be due to the greater ionic radius of  $\text{Fe}^{+3}$  with decrease  $\text{Mn}^{+2}$  ions that caused increase of lattice constant induced in the doped samples.

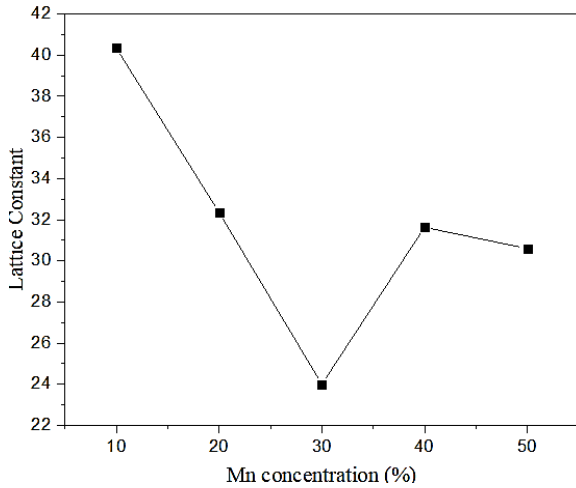


Fig. 3. Lattice constant, (a) of Mn doped bismuth Ferrite dependency upon the extension of Mn concentration

The William plot of all BFO samples is shown in fig.4. In order to estimate the slope of linear fit data plotted against  $\beta \cos \theta$  vis.  $4 \sin \theta$ , gives the information about the inverse of intercept and lattice strain gives the value of crystalline size ( $D_{W-H}$ ) for all the BFO samples. The particle size and lattice strain of Mn doped BFO samples were calculated from the broadening of the XRD peaks

using Williamson-Hall method from the following relation[12].

$$\beta \cos \theta = \frac{k}{D} + 4\epsilon \sin \theta \quad (9)$$

Here,  $\beta$  is represented the integral breadth in radian,  $\theta$  is the Bragg angle,  $k$  is the shape value 0.94,  $D$  is the William hall particles size ( $D_{H-W}$ ) and  $\epsilon$  stand for micro slop. The calculated lattice strains from W-H plot were found be increase with increasing Mn-concentration which is presented in Table 2.

Table 2. Mn Concentration, Crystalline Size (DW-H) and strain of Mn doped BFO ferrites

Mn contents	Particle size ( $D_{W-H}$ )	Strain
10%	270.87	0.000377
20%	234.59	0.00372
30%	277.59	0.00378
40%	398.0	0.00391
50%	275.5	0.00377

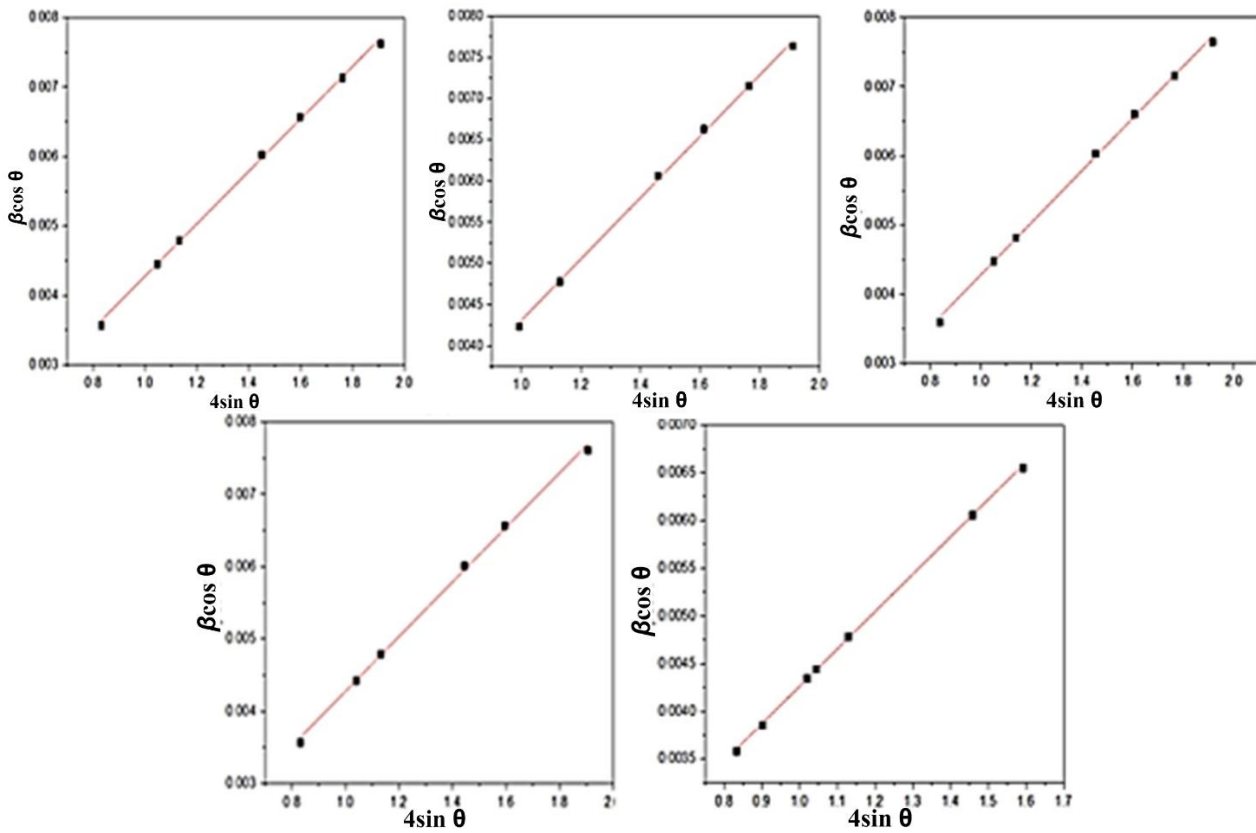


Fig. 4. Hall-Williamson plot of BFO having Mn Content (a)10% (b) 20% (c) 30% (d) 40% (e) 50% (color online)

The sign of slope is due to the nature of strain. Positive slope is indicated to tensile strain whereas the negative slope corresponds to the compressive slope. Fig. 4 shows that the

average crystalline size is increases with the Mn doping from 10% to 50% of BFO samples. The crystallite size is

increased due higher strain as the loss of even one oxygen creates high strain [13].

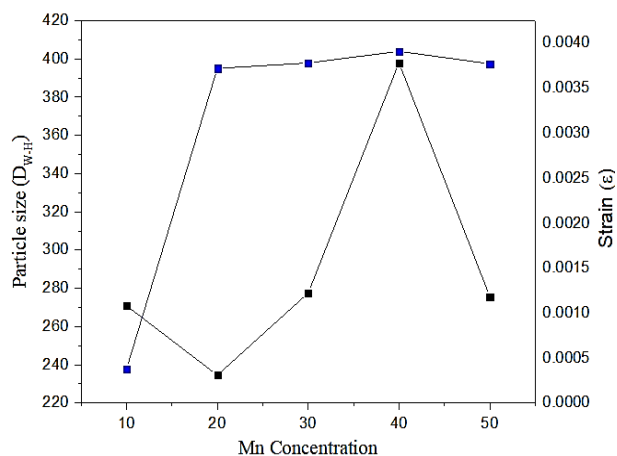


Fig. 5. Variation of average crystallite size (W-H) and induced strain with Mn concentration

SEM was used in the microstructural analysis of the specimens. The specimens were analyzed for grain size and morphology. The SEM micrographs of Mn-doped BFO clearly show in Fig. 6 that there was inhomogeneous distribution of various sizes and morphology [14]. The formation of nanorods of various sizes were seen [15]. The formation of nanorods might enhance the usability of bismuth ferrite samples. There was a significant change in BiFeO<sub>3</sub> morphology by the addition of Mn atoms into the bismuth ferrite. The average grain size was 19.48nm, 21.50 nm and 27.50 nm for 30%, 40% and 50% Mn-doped BFO respectively. The change in morphology increased with the increase in amount of Manganese in BiFeO<sub>3</sub> samples [16].

Bismuth ferrite is studied as a potential material applied in photocatalytic degradation of some organic pollutants or as a photocatalyst for water splitting due to its relatively narrow gap [17]. UV-Vis absorption calculations along with the band gap measurements with 30% concentration of Mn doped BFO is appeared in Fig. 7. Calculated band gap value was 1.77eV approximately. An abrupt absorption characteristic peak at 385nm for bismuth ferrite samples was examined [18]. The optical properties of synthesized samples were finalized in the 200-1000nm of wavelength. When comparing pure BFO specimen to doped MnBFO, A prominent red shift can be examined in the absorption spectra of the doped samples in respect to a broader range of visible light [16].

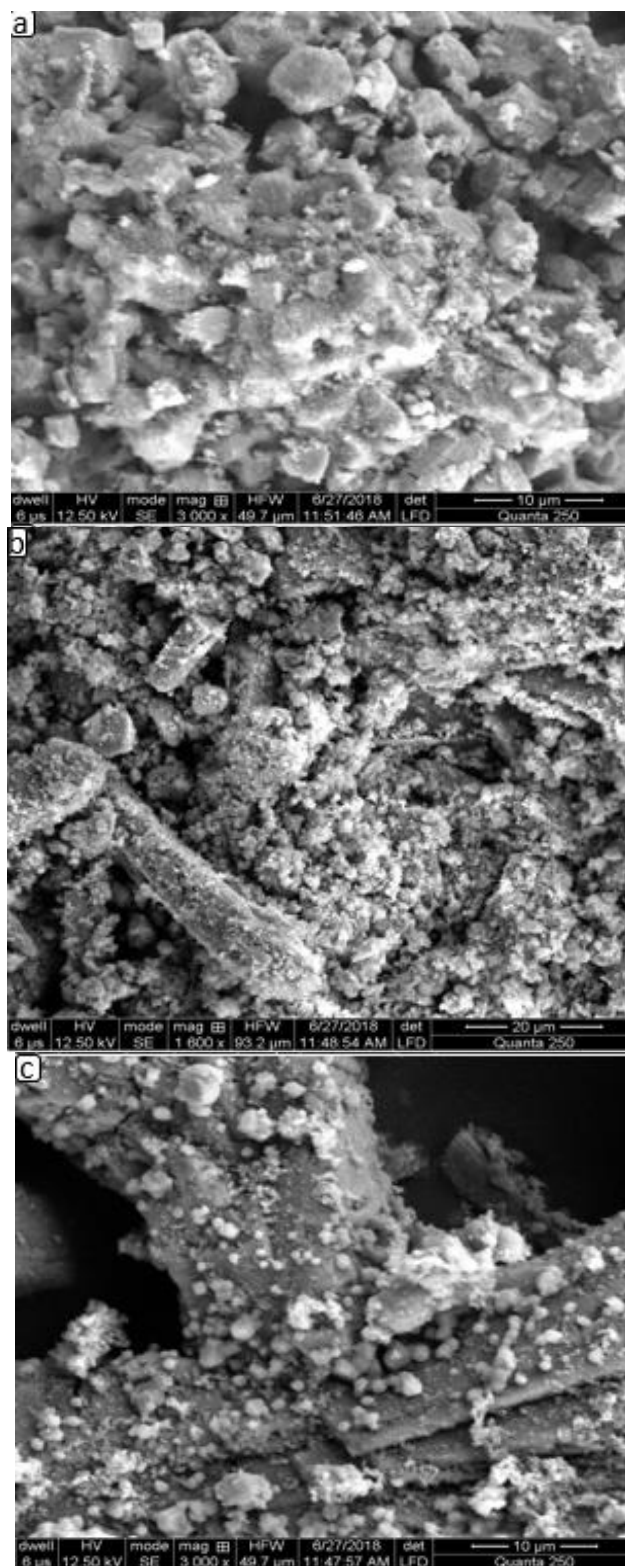


Fig. 6. SEM micrographs of Mn doped BFO with (a) 30% (b)40% (c)50%

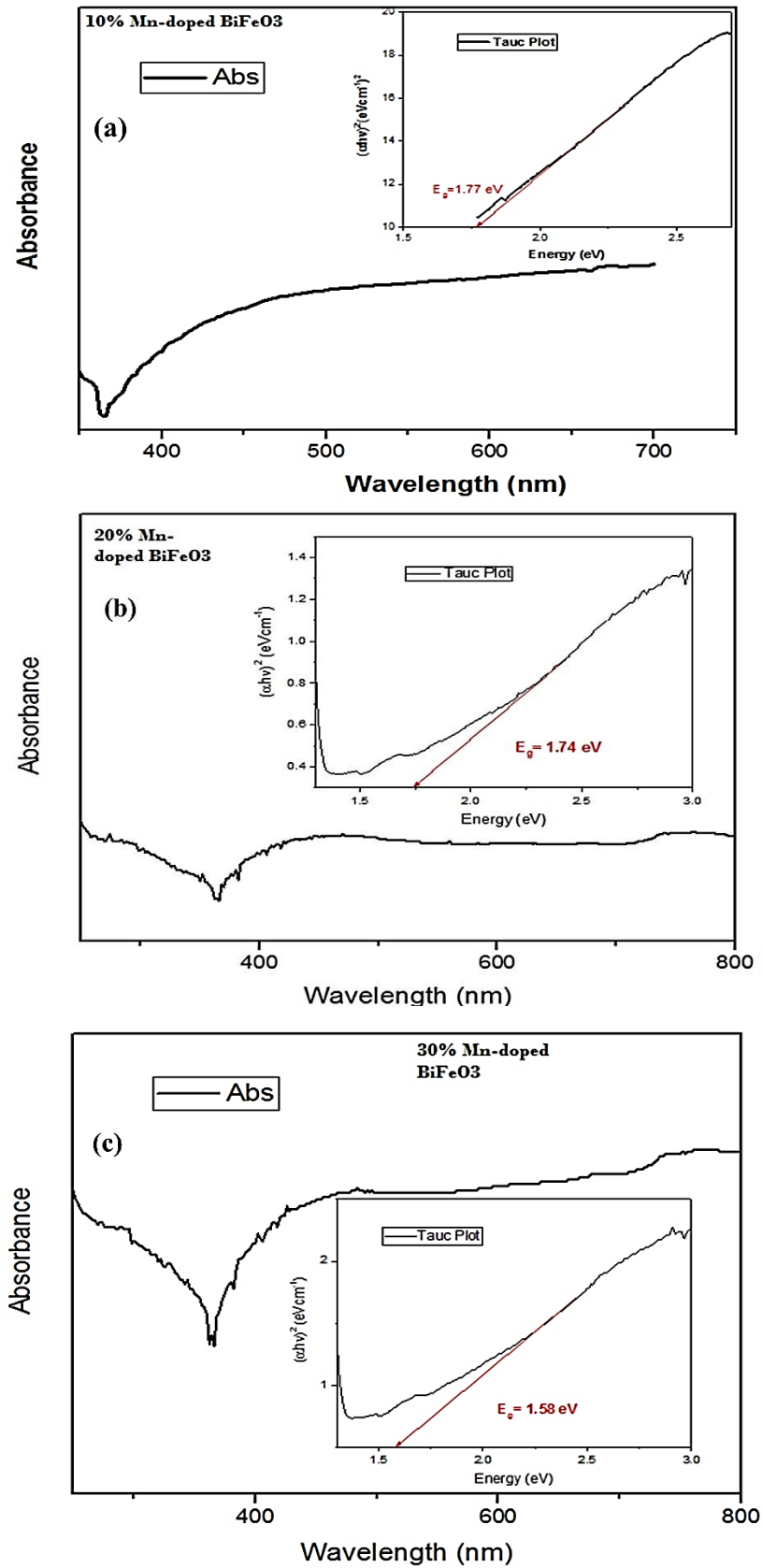


Fig. 7. UV-Visible Absorption Spectra of Mn-doped BFO (a) 10% (b) 20% and (c) 30% (color online)

UV-Vis absorption calculations along with the band gap measurements indicate that bismuth ferrite samples

can absorb more light than Mn-doped BiFeO<sub>3</sub> samples. UV-Vis absorption calculations along with the band gap

measurements with 40% concentration of Mn doped BFO is appeared in Fig. 7. Calculated band gap value was 1.74eV approximately. The absorption spectrum of wavelength was calculated at 380nm. Using Tauc's equation, energy band gap of doped samples can be calculated through the tangent line in the plot of  $(\alpha h\nu)^n$

$$(\alpha h\nu) = k(h\nu - E_g)^n \quad (10)$$

" $\alpha$ " is absorbance coefficient, " $h\nu$ " is the incident photon energy, " $k$ " is energy independent constant while " $E_g$ " is the energy gap of the optical band. UV-Vis absorption calculations along with band gap measurements with 50% concentration of Mn doped BFO is shown in Fig. 3. Estimated band gap values were 1.58eV. It has been clearly found that BFO's band gap decreased as MN in BFO samples increased. Band gap of Mn doped BFO ferrites with corresponding wavelength have shown in below Table 3.

Table 3. Mn doped BFO ferrites

Mn content (%)	Absorption wavelength (nm)	Band gap (eV)
30	385	1.77
40	380	1.74
50	378	1.58

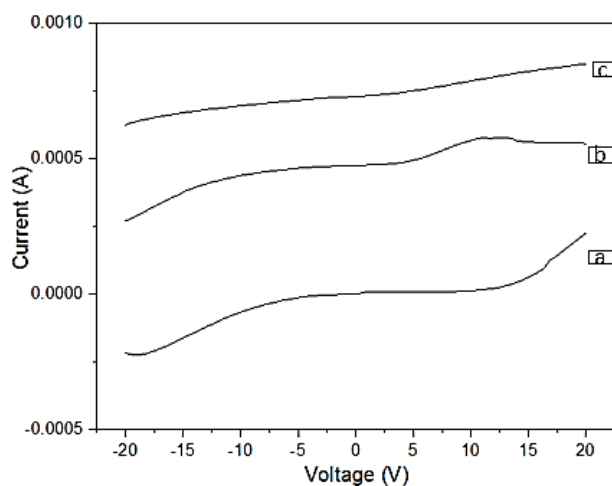


Fig. 8. I-V Characteristics of Mn doped BFO

Fig. 8 (a-b-c) shows I - V curves for Mn doped Bismuth ferrites with biasing voltage (0  $\rightarrow$  +20 V and 0  $\rightarrow$  -20 V). The current is almost linearly increasing to a certain voltage (15V) and nonlinear is dominant at higher biasing voltage. The nature of I - V curves at forward bias (0  $\rightarrow$  +20V) and reverse bias (0  $\rightarrow$  -20V) showed identical behavior. However, as doping is increased, I - V curves showed two remarkable changes. Due to presence of dopant element, first immediate enhancement of current magnitude is observed. The magnitude of I - V curve gradually decreases on further increment of dopant element. In Fig. 4 (a) at 10V, current is gradually

increased but voltage remains constant. In the material characteristics I-V, the typical characteristic of a decrease in the current and the increase in the bias voltage is known as negative difference resistance (NDR) effect. The fundamental characteristics of I - V curves in our measurement are not significantly modified, although minor differences are observed due to doping of manganese in BFO ferrites

#### 4. Conclusion

At low temperature (80°C) pure Mn-doped BiFeO<sub>3</sub> nano-powder multiferroic phase has been prepared using co-precipitation process. Bi<sub>2</sub>O<sub>3</sub> was an important precursor to prevent impure and additional phases. Nano-crystalline particles of ferrites were effectively synthesized via Coprecipitation technique. XRD and FTIR analysis showed Sharp crystalline peaks of Mn doped BiFeO<sub>3</sub> displayed the development of the perovskite-based rhombohedral structure. The result of XRD showed that the small lattice distortion or phase change appeared due to the shifting of peaks to some higher angle in BiFeO<sub>3</sub> samples while increasing the Mn content. We report irregular variation in average crystal size, increase in lattice constant and a gradual decrease in volume of unit cell. SEM analysis demonstrate the change in morphology of samples increases with increasing concentration of manganese in BiFeO<sub>3</sub> samples. It was estimated through UV-vis spectroscopy that energy band gap is decreases as the amount of dopant element Mn is increased. It was noticed in I-V characteristics curve that due to presence of dopant element abrupt enhancement of current magnitude is observed. The magnitude of I - V curve gradually decreases on further increase of amount of manganese.

#### Acknowledgements

This work was supported by the Higher Education Commission (HEC) of Pakistan [Grant No: 8615/Punjab/NRPU/R&D/HEC/2017].

#### References

- [1] Y.-W. Fang, H.-C. Ding, W.-Y. Tong, W.-J. Zhu, X. Shen, S.-J. Gong, X.-G. Wan, C.-G. Duan, Science Bulletin **60**, 156 (2015).
- [2] V. Khomchenko, D. Kiselev, J. Vieira, L. Jian, A. Kholkin, A. Lopes, Y. Pogorelov, J. Araujo, M. J. Maglione, Journal of Applied Physics **103**, 024105 (2008).
- [3] M. Fiebig, T. Lottermoser, D. Fröhlich, A. V. Goltsev, R.V. Pisarev, Nature **419**, 818 (2002).
- [4] R. Seshadri, N. A. Hill, Chemistry of materials **13**, 2892 (2001).

- [5] S. Chauhan, M. Kumar, S. Chhoker, S. Katyal, H. Singh, M. Jewariya, K. J. Yadav, *Solid State Communications* **152**, 525 (2012).
- [6] C. M. Cho, J. H. Noh, I. S. Cho, J. S. An, K. S. Hong, J. Y. Kim, *Journal of the American Ceramic Society* **91**, 3753 (2008).
- [7] N. Zhang, Q. Wei, L. Qin, D. Chen, Z. Chen, F. Niu, J. Wang, Y. J. J. O. N. Huang, *Journal of Nanoscience and Nanotechnology* **17**, 544 (2017).
- [8] S. Pradhan, J. Das, P. Rout, V. Mohanta, S. Das, S. Samantray, D. Sahu, J.-L. Huang, S. Verma, B. J. Roul, *Journal of Physics and Chemistry of Solids* **71**, 1557 (2010).
- [9] G. Dong, G. Tan, Y. Luo, W. Liu, A. Xia, H. J. Ren, *Applied Surface Science* **305**, 55 (2014).
- [10] D. Kothari, V. R. Reddy, A. Gupta, D. Phase, N. Lakshmi, S. Deshpande, C. M. Awasthi, *Journal of Physics: Condensed Matter* **19**, 136202 (2007).
- [11] J. Silva, A. Reyes, H. Esparza, H. Camacho, L. J. Fuentes, *Integrated Ferroelectrics* **126**, 47 (2011).
- [12] S. Chandel, P. Thakur, M. Tomar, V. Gupta, A. J. Thakur, *Ceramics International* **43**, 13750 (2017).
- [13] M. Abushad, W. Khan, S. Naseem, S. Husain, M. Nadeem, A. Ansari, *Ceramics International* **45**, 7437 (2019).
- [14] H. M. Xu, H. Wang, J. Shi, Y. Lin, C. Nan, *Nanomaterials* **6**, 215 (2016).
- [15] C. H. Yang, D. Kan, I. Takeuchi, V. Nagarajan, J. Seidel, *Physical Chemistry Chemical Physics* **14**, 15953 (2012).
- [16] Y. Zhang, Y. Wang, J. Qi, Y. Tian, M. Sun, J. Zhang, T. Hu, M. Wei, Y. Liu, J. Yang, *Nanomaterials* **8**, 711 (2018).
- [17] V. Srinivas, A. Raghavender, K. V. Kumar, *Physics Research International* **2016**, 4835328 (2016).
- [18] P. Kumar, M. Kar, *Materials Science*, arXiv preprint arXiv, (2014).

---

\* Corresponding author: khuram\_uaf@yahoo.com